Journal of Nuclear Medicine, published on February 9, 2016 as doi:10.2967/jnumed.115.169342

Biodistribution and radiation dosimetry of the anti-HER2 Affibody molecule ^{68}Ga-ABY-025 in breast cancer patients

Mattias Sandström[1], Karolina Lindskog[1], Irina Velikyan[1], Anders Wennborg[2], Joachim Feldwisch[2,3], Dan Sandberg[1],Vladimir Tolmachev[3], Anna Orlova[3], Jens Sörensen[1], Jörgen Carlsson[3], Henrik Lindman[4] and Mark Lubberink[1]

[1] Nuclear Medicine and PET, Department of Surgical Sciences, Uppsala University, Uppsala, Sweden.

[2] Affibody AB, Solna, Sweden.

[3] Biomedical Radiation Sciences, Rudbeck Laboratory, Department of Immunology, Genetics and Pathology, Uppsala University, Uppsala, Sweden.

[4] Section of Oncology, Department of Immunology, Genetics and Pathology, Uppsala, Sweden.

Short title: Dosimetry of ^{68}Ga-labelled ABY-025

Corresponding author: Mattias Sandström, Medical Physics, Uppsala University Hospital, SE-75185, Uppsala, Sweden. Telephone: +46186112749. E-mail: mattias.sandstrom@akademiska.se

Key words: Affibody, breast cancer metastases, dosimetry, HER2-receptor, ^{68}Ga-gallium

Word count: 3094

Funding: This work was sponsored by The Swedish Cancer Society (Cancerfonden) and The Swedish Breast Cancer Foundation (Bröstcancerfonden). Affibody AB donated ABY-025.

ABSTRACT

Rationale: ^{68}Ga-ABY-025 is a radiolabelled Affibody molecule for in vivo diagnosis of HER2 positive breast cancer tumours with positron emission tomography (PET). The aim of the present work was to measure biodistribution and estimate radiation dosimetry of ^{68}Ga-ABY-025 for two different peptide mass doses in a single group of patients using dynamic and serial whole-body PET/CT.

Methods: Eight patients with metastatic breast cancer were included. Each patient underwent an abdominal 45 min dynamic and three whole-body PET/CT scans at 1, 2 and 4 h after injection of low peptide dose (LD) and high peptide dose (HD), with approximately the same amount of radioactivity, in separate investigations one week apart. As input to the absorbed dose calculations volumes of interest were drawn in all clearly identifiable source organs liver, kidneys, spleen, descending aorta and upper large intestine. Absorbed doses were calculated using Olinda/EXM 1.1.

Results: Of the major organs, the highest radionuclide uptake at 1, 2 and 4 h p.i. was observed in the kidneys and liver. The highest absorbed organ doses were seen in kidneys followed by liver for both LD and HD ^{68}Ga-ABY-025. Absorbed doses to liver and kidneys were slightly but significantly higher for LD. Total effective dose was 0.030 ± 0.003 mSv/MBq for LD and 0.028 ± 0.002 mSv/MBq for HD.

Conclusion: Effective dose for a typical 200 MBq administration of ^{68}Ga-ABY-025 is 6.0 mSv for LD and 5.6 mSv for HD. Therefore, from a radiation dosimetry point of view, HD is preferred

for PET/CT evaluation of HER2-expressing breast cancer tumours. These effective doses are somewhat higher than earlier published values for other ^{68}Ga-labelled tracers, for example 0.021 ± 0.003 mSv/MBq for ^{68}Ga- DOTATATE and ^{68}Ga-DOTATOC, mainly due to higher uptake in liver and kidney.

INTRODUCTION

For women, breast cancer is currently the most common cancer. Human epidermal growth factor receptor 2 (HER2) is overexpressed in about one out of six cases (*1-3*) at initial diagnosis and is associated with poor survival (*1, 3*). Treatments targeted to HER2, such as with the anti-HER2 antibody trastuzumab, have considerably improved the overall survival (*1, 3, 4*). Today, assessment of HER2 status is based on tumor biopsies. However, HER2 expression can vary between the primary tumor and metastases in up to 40% of cases (*2, 5, 6*) and metastatic HER2 expression can change over time, which could necessitate a change of therapy (*7, 8*). Follow-up using biopsies cannot always be performed due to practical reasons or patient discomfort.

Molecular imaging using single photon emission computed tomography (SPECT) and positron emission tomography (PET) might be a noninvasive, whole body based, way to evaluate the HER2 expression quantitatively. One such approach is the use of trastuzumab labeled with ^{111}In ($t_{1/2}$ 2.8 days) (*9*) or ^{89}Zr ($t_{1/2}$ 3.3 days) (*10*) for use with SPECT and PET, respectively, but the slow kinetics of antibodies require imaging several days after administration. One promising way of fast, safe and accurate imaging that specifically binds to a site on the receptor not occupied by current targeting therapeutic drugs (*11-13*) is to use the Affibody molecule ABY-025. ABY-025 labelled with ^{111}In used with SPECT has shown promising clinical results (*14*) which might be further improved today when semi-quantitative standardized uptake value (SUV) SPECT becomes available. The use of PET and ABY-025 labelled with ^{68}Ga ($t_{1/2}$ 68 min) has the potential to provide higher sensitivity, higher resolution images with lower absorbed and effective dose. The use of a short-lived positron emitter, combined with the higher sensitivity of PET and the much faster kinetics of ABY-025 compared to trastuzumab, will allow for imaging

of the tumors within hours after injection instead of days, improving patient comfort and logistics. Tumor to background ratio, and hence detectability of tumors may be dependent on the total amount of peptide injected, since the number of occupation sites might be much higher in tumor sites. Hence the target receptors in normal organs can be saturated while the receptors in tumors are not. A preclinical study has previously indicated that it is possible to discriminate between low and high HER2-expression using Affibody molecules with low specific radioactivity (*15*). Such discrimination has also been indicated in a clinical (*14*) and a preclinical study (*16*) considering the fast clearance of radioactivity from low HER2-expressing tumors.

^{68}Ga-ABY-025 and PET has, in a recent study, shown to be able to discriminate HER2-positive metastases, with SUV correlating well with HER2-expression (*17*). In this study, two different amounts of peptides were administered, with the higher peptide dose giving the best results in terms of detectability and discrimination. The aim of the present work was to measure biodistribution and estimate radiation dosimetry of ^{68}Ga-ABY-025 in a single group of patients injected with two different peptide doses, but approximately the same amount of radioactivity, using dynamic and serial whole-body PET/CT.

MATERIALS & METHODS

Patients

Eight female patients diagnosed with metastatic breast cancer were included in the present work. The study was an academically sponsored clinical trial (trial identifiers EudraCT 2012-005228-14 and NCT01858116), approved by the Regional Board of Medical Ethics and the Swedish Medical Products Agency. All patients signed an informed consent prior to inclusion in the study.

Radiochemistry

Good manufacturing practice compliant production of ^{68}Ga-ABY-025 (*18*) was conducted using a fractionation method (*19*). ^{68}Ga was obtained from a ^{68}Ge/^{68}Ga-generator (IGG100, Eckert & Ziegler). ^{68}Ga-ABY-025 was prepared in two peptide doses (low (LD): 78±8 µg and high (HD): 427±19 µg) with amounts of radioactivity in the same range, hence resulting in an approximately six-fold difference in specific radioactivity values.

PET protocol

PET data were acquired using a Discovery ST (GE Healthcare, Waukesha, WI) PET/CT scanner. After a low-dose CT for patient positioning and attenuation correction, a 45 min dynamic PET scan (6 x 10, 4 x 60, 5 x 180, 5 x 300 s) over the abdominal region was started simultaneously with intravenous injection of 215 ± 58 (range, 124-294) MBq of LD ^{68}Ga-ABY-025. This was followed by three whole-body scans (proximal femur to base of skull) starting at 1, 2 and 4 h after injection, with scan durations of 3, 4 and 5 min per bed position, respectively, each preceded by a low-dose CT examination. Images were reconstructed using normalisation and attenuation-weighted ordered subsets expectation maximisation (OSEM; 2 iterations, 21 subsets) including

all appropriate corrections and a 5.4 mm Gaussian post-filter. Venous blood samples were drawn after each whole body scan for measurement of whole blood radioactivity concentrations. Patients were allowed to urinate between the dynamic scan and each consecutive whole body scan. Urine was collected, weighted, and radioactivity concentration was measured. Accurate cross-calibration between PET/CT, dose calibrator and well counters used to measure blood and urine activity was verified on a monthly basis and was always within 3%. The scan procedure was repeated one week later using 241 ± 49 (range, 159-297) MBq of HD ^{68}Ga-ABY-025.

Volumes of interest

Volumes of interest (VOI) were drawn in the whole-body images and in the last time frame of the dynamic image series over subsets of all clearly identifiable source organs liver, kidneys, spleen, and upper large intestine. VOIs drawn in the last frame of the dynamic scans were transferred to all earlier time frames. In addition, 70% isocontour regions of interest (ROIs) were drawn over 10 planes in first-pass images of the descending aorta and combined to a VOI, and transferred to all later dynamic time frames. Activity concentration and SUV normalized to body mass and injected amount of radioactivity were determined using the mean activity concentration in the VOIs. From these data time-activity curves (TACs) for these organs were computed. A whole-blood TAC was computed by combining the descending aorta TAC based on the dynamic scan with venous blood sample data taken after each whole-body scan.

Absorbed dose calculations

As in peptide receptor radionuclide therapy with ^{177}Lu-octreotate (*20*) red marrow radioactivity concentration was assumed to be equal to blood radioactivity concentration. Total organ activity was calculated by multiplication of the radioactivity concentrations with the organ weights of the

adult reference female phantom (*21*) scaled by the total patient weight. Urinary bladder content was estimated based on linear interpolation between decay-corrected measured amounts of excreted radioactivity, assuming complete voiding. After the last scan, a 4 h voiding interval with filling rates equivalent to those prior to the last measured urine sample was assumed. Time-integrated activity curves of the organ (TACs) were calculated by trapezoidal integration until the last scan, followed by a single-exponential fit to the last three data points extrapolated to infinity. Residence times were obtained by dividing the time-integrated activity by the injected amount of activity. Small intestine, upper large intestine and lower large intestine residence times were estimated using the ICRP 30 gastrointestinal tract model (*22*) based on the measured uptake in the upper large intestine. Remainder of the body activity was calculated as the injected activity minus the sum of the activity in all source organs and the activity excreted to urine up to each measurement point. Absorbed doses were calculated using OLINDA/EXM 1.1 (*23*).

Statistical analysis

Differences between residence times and absorbed doses for both peptide masses were assessed using a Wilcoxon signed-rank test included in the GraphPad Prism (version 6.02) software.

RESULTS

Figure 1 shows typical whole-body images of a single patient for both peptide masses with clear reduction of hepatic radioactivity uptake for the HD. Figure 2 shows the biodistribution, in terms of SUV and percentage of injected activity per organ, for LD and HD. Of the major organs, the highest SUV at 60-240 min after injection was observed in the kidney, followed by liver. Figure 3 shows a direct comparison of the SUV in kidney and liver for LD versus HD. Initial uptake in the liver was higher for LD whilst clearance appeared similar for LD and HD, resulting in a higher residence time ($p<0.05$). For the kidney, a smaller difference in the same direction was found, whereas blood clearance was faster for LD. Residence times, as shown in Table 1, considering mean data from the eight patients, where highest for liver, followed by the kidneys.

Absorbed dose estimates are shown in Table 2. The highest absorbed organ doses were seen in kidney and liver. Figure 4 compares residence times and absorbed doses in kidney and liver, as well as effective dose, for each individual patient.

Total effective dose was 0.030 ± 0.002 mSv/MBq for LD and 0.028 ± 0.003 mSv/MBq for HD. These values would result in an effective dose of 6.0 and 5.6 mSv for a typical administration of about 200 MBq as used in the present study.

Absorbed doses to kidney, liver, gallbladder wall and total body were significantly higher for LD whereas red marrow absorbed dose was significantly higher for HD (Wilcoxon test, $p<0.05$), although mean absolute differences were very small for gallbladder wall (1%), total body (2%), and red marrow (2%).

DISCUSSION

To our knowledge, the present work is the first study of the radiation dosimetry of ^{68}Ga-ABY-025. Radiation absorbed doses were estimated using a protocol combining dynamic PET and serial whole-body PET scans in eight evaluable patients. An effective dose of 3.0 mSv and 2.8 mSv for LD and HD, respectively, will be achieved for a 100 MBq administration, which may be sufficient for clinical use. The administration of about 200 MBq, as in the present study, would give an effective dose in the range 5-6 mSv. These values are considerably lower than the effective dose of 21 mSv calculated for the administration of 200 MBq ^{111}In-ABY-025 in a previous investigation (*14*) and also lower compared to typical FDG-PET examinations, which often give effective doses of around 7 mSv. However, these dose estimates are higher than earlier published values of 0.021 ± 0.003 for ^{68}Ga-DOTATATE and ^{68}Ga-DOTATOC, because of higher uptake in liver and kidney. Another positron-emitting radiometal that has been used for labelling of larger molecules is ^{89}Zr. However, the use of ^{89}Zr is mainly preferred for tracers with slow kinetics, such as antibodies, because of its long radioactive half-life (3.3 days). This longer half-life inherently results in higher effective doses, for example 0.55 ± 0.07 mSv/MBq for ^{89}Zr-ibritumomab tiuxetan (*24*). For the present patient group, the absorbed doses due to ^{68}Ga-ABY-025 should also be seen in the perspective that diagnostic CT-scans of the thorax and abdomen will give comparable or higher effective doses. In addition, many patients will undergo radiation treatment, leading to much higher radiation doses.

The use of a combined dynamic – whole body protocol allows for detailed assessment of the TACs of pre-defined risk organs, while improving patient comfort by allowing patients to leave the scanner between subsequent whole-body scans. The use of a 45 min dynamic scan has the

disadvantage of not being able to follow other risk organs during this time. However, based on earlier studies with this compound (*14*) it was well known that the main source and risk organs were the liver and the kidneys. Since both of these can be imaged in one bed position the advantage of being able to image these organs over 45 min exceeded the disadvantage of not being able to image other risk organs during this time.

Absorbed doses in kidneys and liver were slightly higher for LD than for HD, and the same was observed for the effective dose. The differences in effective dose were minor even within individual patients. The organ receiving the highest absorbed radiation dose was the kidney followed by the liver. The absorbed dose to these organs, after a 100 MBq administration, will be approximately 40 mGy and 15 mGy for for kidney and liver, respectively, which is less than the maximum allowed absorbed dose of 50 mGy to a single organ in an healthy adult research subject (*25*).

Since the scan protocol covered the major part of the radioactive decay of ^{68}Ga, the remainder of the decay after the last scan amounts to at most a small percentage of the total number of disintegrations in each organ. Therefore, the uncertainty in extrapolation after the 4 h whole-body scan only has minor effects on the total estimate of the time-integrated activity.

The patients included in the present work all had breast cancer tumours and metastases with varying degree of HER2 expression, which is not accounted for in Olinda/EXM 1.1 calculations to assess radiation dosimetry. However, the tumour burden was limited, and since the major part of the absorbed dose to adrenal glands, kidneys and healthy liver tissue is due to locally absorbed

beta radiation, taking into account cross-dose from tumours to healthy tissues would have resulted in negligible changes in organ doses.

CONCLUSION

The effective dose for a typical 200 MBq administration of ^{68}Ga-ABY-025 was found to be 6.0 mSv for LD (78±8 µg) and 5.6 mSv for HD (427±19 µg) of ^{68}Ga-ABY-025. The absorbed doses to kidneys and liver were lower for the HD than LD. Assuming that the tumour uptake was unaffected by peptide dose, these results suggest higher tumour to background contrast for HD. Therefore, in terms of biodistribution and dosimetry, HD is preferred in the diagnosis and pre-treatment HER2-status evaluation of breast cancer patients.

ACKNOWLEDGEMENT

The authors want to thank Mimmi Lidholm, Annie Bjurebäck, Maj Wiberg, Lars Lindsjö, Mirtha Ponce Zoto and Marie Åhlman for their technical assistance in performing the scans. This work was sponsored by The Swedish Cancer Society (Cancerfonden) and The Swedish Breast Cancer Foundation (Bröstcancerfonden). Affibody AB donated ABY-025.

REFERENCES

1. Cortes J, Fumoleau P, Bianchi GV, et al. Pertuzumab monotherapy after trastuzumab-based treatment and subsequent reintroduction of trastuzumab: activity and tolerability in patients with advanced human epidermal growth factor receptor 2-positive breast cancer. *J Clin Oncol.* 2012;30:1594-1600.

2. Houssami N, Macaskill P, Balleine RL, Bilous M, Pegram MD. HER2 discordance between primary breast cancer and its paired metastasis: tumor biology or test artefact? Insights through meta-analysis. *Breast Cancer Res Treat.* 2011;129:659-674.

3. Verma S, Miles D, Gianni L, et al. Trastuzumab emtansine for HER2-positive advanced breast cancer. *N Engl J Med.* 2012;367:1783-1791.

4. Slamon DJ, Leyland-Jones B, Shak S, et al. Use of chemotherapy plus a monoclonal antibody against HER2 for metastatic breast cancer that overexpresses HER2. *N Engl J Med.* 2001;344:783-792.

5. Aurilio G, Disalvatore D, Pruneri G, et al. A meta-analysis of oestrogen receptor, progesterone receptor and human epidermal growth factor receptor 2 discordance between primary breast cancer and metastases. *Eur J Cancer.* 2014;50:277-289.

6. Wilking U, Karlsson E, Skoog L, et al. HER2 status in a population-derived breast cancer cohort: discordances during tumor progression. *Breast Cancer Res Treat.* 2011;125:553-561.

7. Karlsson E, Sandelin K, Appelgren J, et al. Clonal alteration of breast cancer receptors between primary ductal carcinoma in situ (DCIS) and corresponding local events. *Eur J Cancer.* 2014;50:517-524.

8. Lindstrom LS, Karlsson E, Wilking UM, et al. Clinically used breast cancer markers such as estrogen receptor, progesterone receptor, and human epidermal growth factor receptor 2 are unstable throughout tumor progression. *J Clin Oncol.* 2012;30:2601-2608.

9. Gaykema SB, de Jong JR, Perik PJ, et al. (111)In-trastuzumab scintigraphy in HER2-positive metastatic breast cancer patients remains feasible during trastuzumab treatment. *Mol Imaging.* 2014;13.

10. Dijkers EC, Oude Munnink TH, Kosterink JG, et al. Biodistribution of 89Zr-trastuzumab and PET imaging of HER2-positive lesions in patients with metastatic breast cancer. *Clin Pharmacol Ther.* 2010;87:586-592.

11. Ahlgren S, Orlova A, Wallberg H, et al. Targeting of HER2-expressing tumors using 111In-ABY-025, a second-generation affibody molecule with a fundamentally reengineered scaffold. *J Nucl Med.* 2010;51:1131-1138.

12. Eigenbrot C, Ultsch M, Dubnovitsky A, Abrahmsen L, Hard T. Structural basis for high-affinity HER2 receptor binding by an engineered protein. *Proc Natl Acad Sci U S A.* 2010;107:15039-15044.

13. Feldwisch J, Tolmachev V, Lendel C, et al. Design of an optimized scaffold for affibody molecules. *J Mol Biol.* 2010;398:232-247.

14. Sörensen J, Sandberg D, Sandstrom M, et al. First-in-human molecular imaging of HER2 expression in breast cancer metastases using the 111In-ABY-025 affibody molecule. *J Nucl Med.* 2014;55:730-735.

15. Tolmachev V, Wallberg H, Sandstrom M, Hansson M, Wennborg A, Orlova A. Optimal specific radioactivity of anti-HER2 Affibody molecules enables discrimination between xenografts with high and low HER2 expression levels. *Eur J Nucl Med Mol Imaging.* 2011;38:531-539.

16. Tolmachev V, Tran TA, Rosik D, Sjoberg A, Abrahmsen L, Orlova A. Tumor targeting using affibody molecules: interplay of affinity, target expression level, and binding site composition. *J Nucl Med.* 2012;53:953-960.

17. Sörensen J, Velikyan I, Sandberg D, et al. Measuring HER2-receptor expression in metastatic breast cancer using [68Ga]ABY-025 Affibody PET/CT. *Theranostics.* 2015:In press.

18. Velikyan I, Wennborg A, Feldwisch J, et al. GMP compliant preparation of a 68Gallium-labeled Affibody analogue for breast cancer patient examination: first-in-man. *European journal of nuclear medicine and molecular imaging.* 2014;41:S228-S229.

19. Velikyan I, Beyer GJ, Langstrom B. Microwave-supported preparation of (68)Ga bioconjugates with high specific radioactivity. *Bioconjug Chem.* 2004;15:554-560.

20. Forrer F, Krenning EP, Kooij PP, et al. Bone marrow dosimetry in peptide receptor radionuclide therapy with [177Lu-DOTA(0),Tyr(3)]octreotate. *Eur J Nucl Med Mol Imaging.* 2009;36:1138-1146.

21. Stabin MG. MIRDOSE: personal computer software for internal dose assessment in nuclear medicine. *J Nucl Med.* 1996;37:538-546.

22. *ICRP Publication 30: Limits for Intakes of Radionuclides by Workers*. Ottawa: International Commission on Radiological Protection; 1980.

23. Stabin MG, Sparks RB, Crowe E. OLINDA/EXM: the second-generation personal computer software for internal dose assessment in nuclear medicine. *J Nucl Med.* 2005;46:1023-1027.

24. Rizvi SN, Visser OJ, Vosjan MJ, et al. Biodistribution, radiation dosimetry and scouting of 90Y-ibritumomab tiuxetan therapy in patients with relapsed B-cell non-Hodgkin's lymphoma using 89Zr-ibritumomab tiuxetan and PET. *Eur J Nucl Med Mol Imaging.* 2012;39:512-520.

25. FDA. Food and Drug Administration Code of Federal Regulations. *CGR.* 1991;21:361.

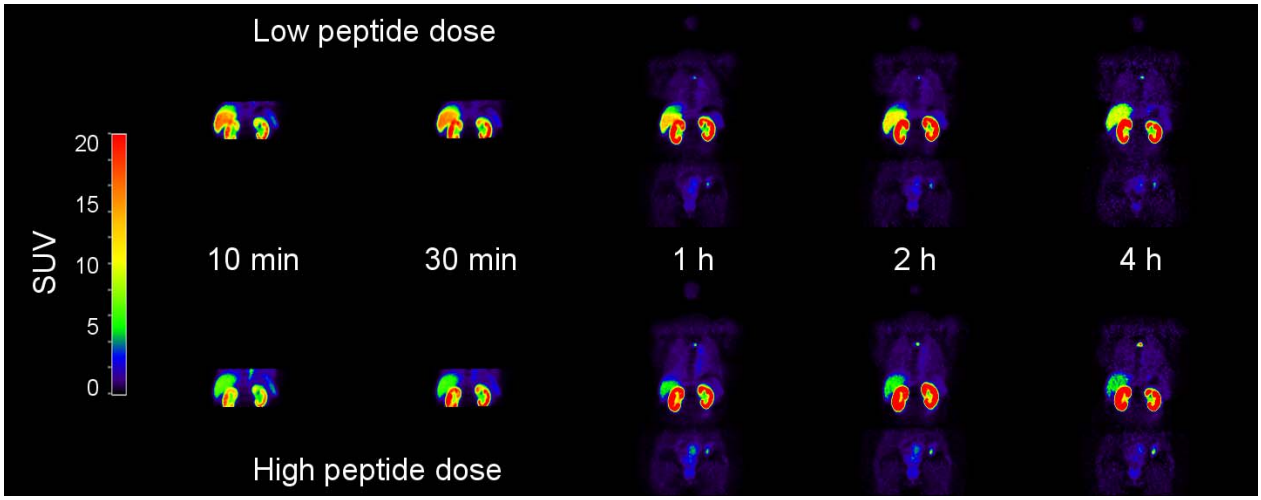

Figure 1 – Representative whole body images at 10, 30, 60, 120 and 240 min p.i. of low peptide mass dose, LD, and high peptide mass dose, HD, in the same patient.

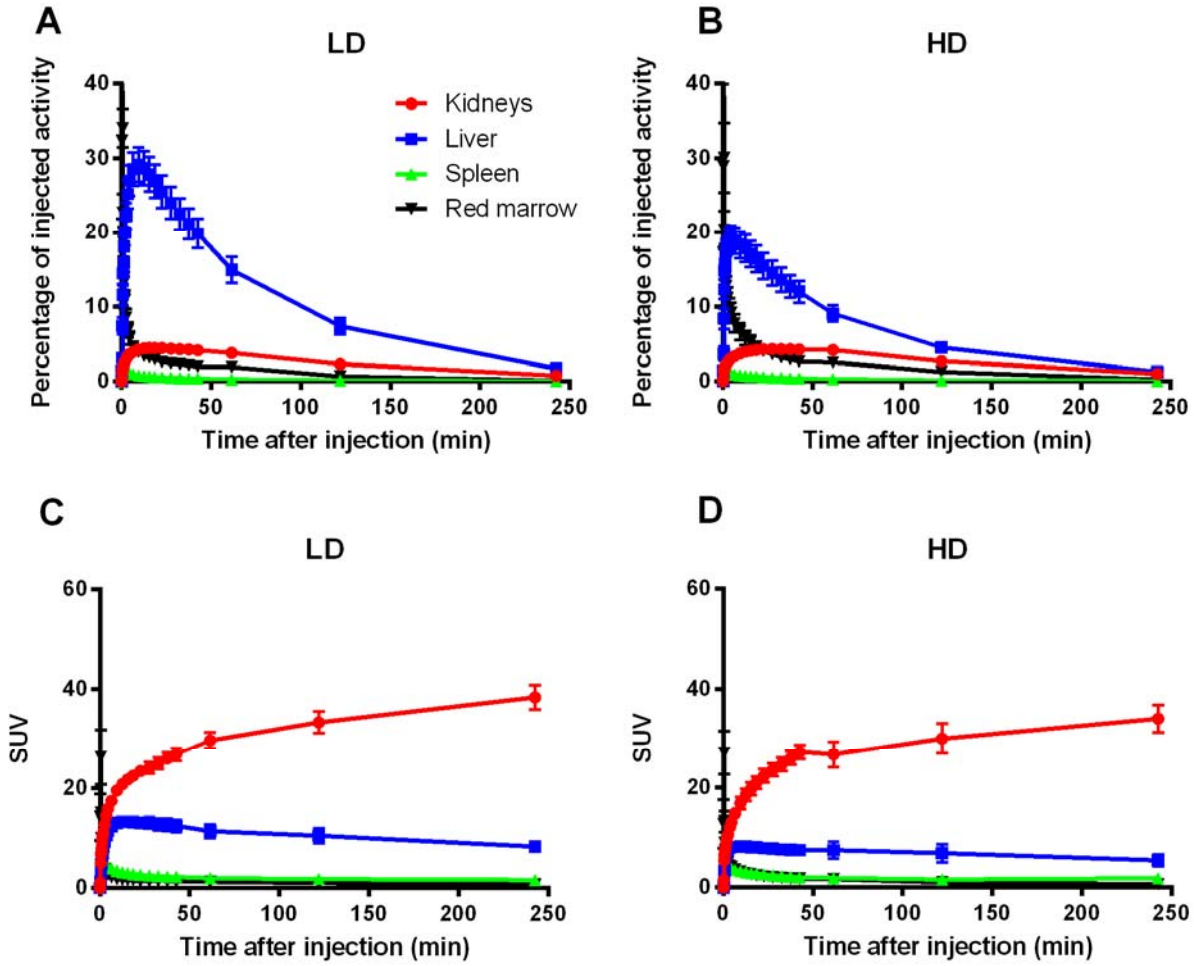

Figure 2 – Percentage of injected activity (A,B) and SUV (C,D) as a function of time after injection in kidneys, liver, spleen and red marrow for LD (A,C) and HD (B,D). Error bars indicate standard deviations. Percentage of injected radioactivity was not corrected for radioactive decay.

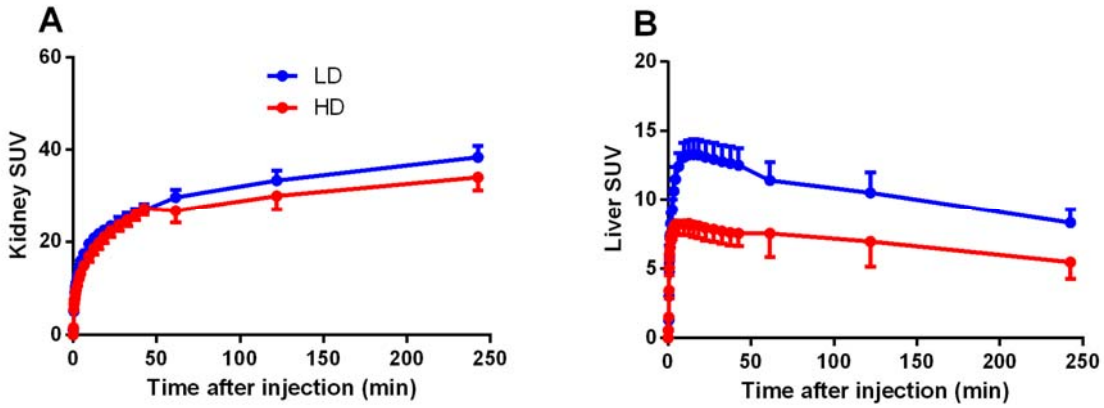

Figure 3 – Direct comparison of SUV in kidney (A) and liver (B) for LD versus HD. Error bars indicate standard deviations.

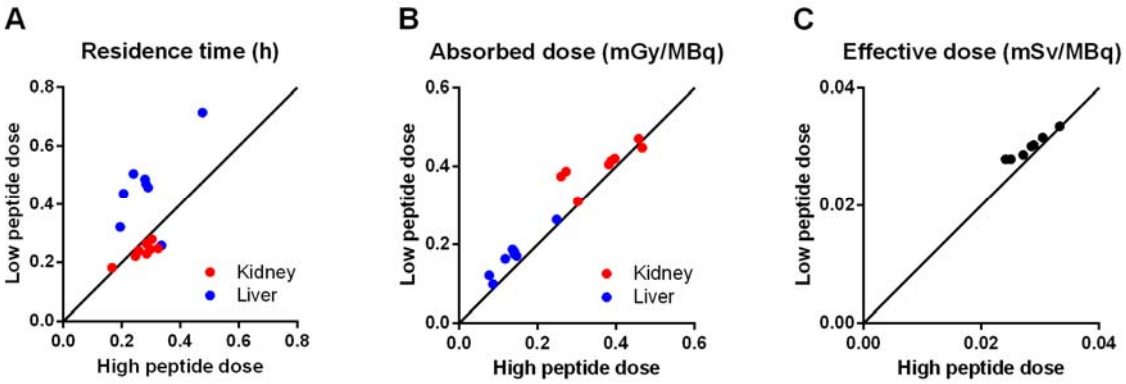

Figure 4 – Residence times (A), absorbed doses (B) in kidney and liver, and effective dose (C) for each patient, shown as LD versus HD. The solid line in each panel is the line of identity between LD and HD.

Table 1 – Residence times (h) (mean ± SD; N=8)

	LD	HD
Kidney*	0.238 ± 0.029	0.216 ± 0.047
Liver*	0.456 ± 0.135	0.366 ± 0.144
Spleen	0.010 ± 0.003	0.009 ± 0.002
Urinary bladder contents	0.004 ± 0.002	0.005 ± 0.002
Bone marrow*	0.028 ± 0.010	0.038 ± 0.014
Heart contents*	0.009 ± 0.003	0.012 ± 0.005
SI contents	0.007 ± 0.002	0.006 ± 0.002
ULI contents	0.002 ± 0.001	0.002 ± 0.001
LLI contents	0.000 ± 0.000	0.000 ± 0.000
Remainder of the body*	0.871 ± 0.140	0.971 ± 0.167

SI: small intestine; ULI: upper large intestine; LLI: lower large intestine
* Significant difference between the peptide masses LD and HD (Wilcoxon signed-rank test; $p<0.05$)

Table 2 – ^{68}Ga-ABY-025 absorbed doses (mGy/MBq) (mean ± SD; N=8)

	LD	HD
Adrenals	0.022 ± 0.001	0.021 ± 0.001
Brain	0.009 ± 0.001	0.010 ± 0.002
Breasts	0.010 ± 0.001	0.011 ± 0.001
Gallbladder Wall*	0.023 ± 0.002	0.022 ± 0.002
LLI Wall	0.012 ± 0.002	0.013 ± 0.002
Small Intestine	0.017 ± 0.002	0.017 ± 0.001
Stomach Wall	0.015 ± 0.003	0.015 ± 0.001
ULI Wall	0.017 ± 0.001	0.017 ± 0.001
Heart Wall*	0.019 ± 0.003	0.022 ± 0.004
Kidney*	0.404 ± 0.049	0.366 ± 0.079
Liver*	0.170 ± 0.049	0.137 ± 0.052
Lungs	0.013 ± 0.001	0.014 ± 0.001
Muscle	0.011 ± 0.001	0.012 ± 0.001
Ovaries	0.012 ± 0.001	0.013 ± 0.002
Pancreas	0.019 ± 0.000	0.019 ± 0.000
Red Marrow*	0.015 ± 0.002	0.017 ± 0.003
Osteogenic Cells	0.021 ± 0.003	0.023 ± 0.004
Skin	0.009 ± 0.001	0.010 ± 0.001
Spleen	0.039 ± 0.008	0.037 ± 0.006
Thymus	0.011 ± 0.001	0.012 ± 0.002
Thyroid	0.010 ± 0.001	0.011 ± 0.002
Urinary Bladder Wall	0.016 ± 0.004	0.018 ± 0.003
Uterus	0.012 ± 0.001	0.013 ± 0.002
Total body*	0.018 ± 0.000	0.018 ± 0.000
Effective Dose Equivalent (mSv/MBq)	0.048 ± 0.004	0.045 ± 0.006
Effective dose (mSv/MBq)	0.030 ± 0.002	0.028 ± 0.003

* Significant difference between the peptide masses LD and HD (Wilcoxon signed-rank test; $p<0.05$)